Design of fixed wing micro air vehicles

P. Cosyn and J. Vierendeels
Department of Flow, Heat and Combustion Mechanics
Ghent University
Belgium

ABSTRACT

The paper describes the methodology and computational design strategies used to develop a series of fixed wing micro air vehicles (MAVs) at the Ghent University. The emphasis of the research is to find an optimal MAV-platform that is bound to geometrical constraints but superior in its performance. This requires a multidisciplinary design optimisation but the challenges are mainly of aerodynamic nature. Key areas are endurance, stability, controllability, manoeuvrability and component integration. The highly three-dimensional low Reynolds number flow, the lack of experimental databases and analytical or empirical models of MAV-aerodynamics required fundamental research of the phenomena. This includes the use of a vortex lattice method, three-dimensional CFD-computations and a numerical propeller optimisation method to derive the forces and their derivatives of the MAV and propeller for performance and stability-related optimisation studies. The design method leads to a simple, stable and robust flying wing MAV-platform that has the agility of a fighter airplane. A prototype, the UGMAV25, was constructed and flight tests were performed. The capabilities of the MAV were tested in a series of successful flight manoeuvres. The UGMAV15, a MAV with a span of 15cm, is also developed to test flight-qualities and endurance at this small scale. With the current battery technology, a flight-time of at least one hour is expected.

NOMENCLATURE

b	wing span
b_c	span ratio
c	blade chord
c_c	chord ratio
g	gravity acceleration
$k\phi$	electromotive force
l_{VT}	distance between AC of tail and wing
m_{bat}	battery mass
m_{rem}	mass of the vehicle without battery
n	turn speed of the propeller (1/s)
n_{mot}	motor turn speed (1/s)
r	local radius
t/c	propeller section thickness ratio
w	local velocity
AR	aspect ratio
B	number of propeller blades
C_{bat}	battery energy density
$C_{d,0}$	zero-lift drag coefficient
$C_{d,blade}$	blade section drag coefficient
$C_{f,lam}$	laminar friction drag of a flat plate
C_l	rolling moment coefficient
$C_{l,blade}$	blade section lift coefficient

Paper No. 3060. Manuscript received 8 December 2005, accepted 12 March 2007.

https://doi.org/10.1017/S0001924000004565 Published online by Cambridge University Press

C_m	pitching moment coefficient
$C_{m,c/4}$	25%-chord pitching moment coeff.
C_D	drag coefficient
$C_{D,vor}$	vortex drag coefficient
C_L	lift coefficient
$C_{L,vor}$	vortex lift coefficient
C_{VT}	vertical tail volume coefficient
D	drag
E	endurance
I	motor current
I_0	no load current
J	advance ratio
K_b	span effectiveness
K_v	vortex lift parameter
L	lift
M	motor torque
M_0	no load friction torque
P_c	dimensionless power
P_{bat}	battery power
P_{dev}	power needed for electronics
Q	propeller torque
Q'	propeller torque per unit radius
R	propeller radius
R_{mot}	motor internal resistance
Re_{blade}	local Reynolds number
Re_p	Reynolds number based on V and R
S	wing surface area
S_{VT}	vertical tail surface area
T	propeller thrust
T'	propeller thrust per unit radius
T_c	dimensionless thrust
U	motor voltage
V	free stream velocity
W	weight
Y_β	side force derivative to side slip
α	angle-of-attack
δ	control surface angle
ε	blade section drag to lift ratio
ϕ	flow angle
η	efficiency of the propulsion system
η_{gear}	gear efficiency
η_{mot}	motor efficiency
η_{prop}	propeller efficiency
λ	speed ratio
μ	dynamic viscosity of air
ρ	air density
Ω	turn speed of the propeller (rad/s)
Ω_0	no load speed
Ω_{mot}	turn speed of the motor (rad/s)

1.0 INTRODUCTION

Small unmanned aerial vehicles and micro air vehicles are at the forefront of current aeronautical research. They were first defined by DARPA (Defence Advanced Research Projects Agency) as six degree-of-freedom machines able to perform a variety of missions[1]. A maximum dimension of 15cm (6 inch) with a payload mass of 18g (0·63oz) was imposed as a first goal but, depending on the missions and payloads, slightly larger MAVs need to be developed which may include electronic equipment such as sensors, an autopilot and a global positioning system. Technological advancements in micro-electronics and MEMS (micro-electromechanical systems) and a multitude of interesting civil and military applications play a big role in the current desire of researchers around the globe to develop this new class of flight vehicle. Missions of interest for fixed wing MAVs are for example surveillance, communications, detection, search and rescue operations and the placement of sensors. Key aspects that drive the need for MAVs are its low cost, transportability, usability and size in comparison to other solutions for a certain task. Besides fixed-wing MAVs[2-4], flapping[5] and rotating[6] wing MAVs are being developed but, primarily for low-speed indoor missions.

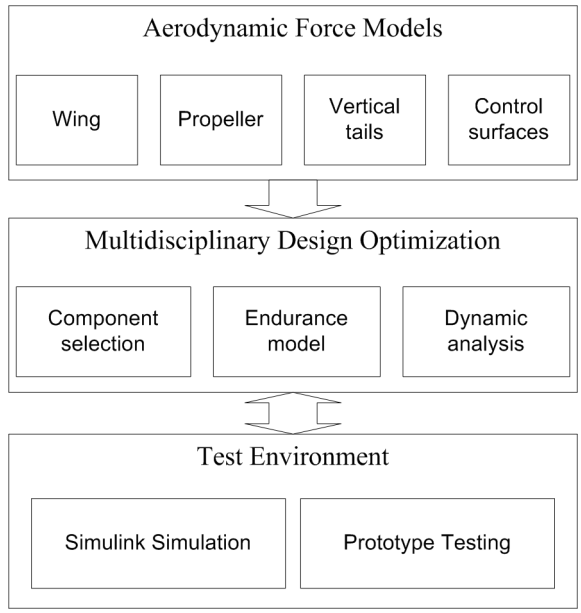


Figure 1. Methodology.

The current research is focused on the design of a fixed wing MAV-platform. The word 'MAV-platform' is used to stress that the MAV is only equipped with the necessary core components of the vehicle, which are its wing structure, propulsion system, energy source, control surfaces and radio- and control equipment needed for flight testing. Payload masses, which may include an autopilot, sensors etc., are added in the form of dummy masses.

The MAVs developed are flying wings (i.e. without a fuselage) using a propeller driven propulsion system. This propulsion choice is obvious as optimal performance is desired and no feasible alternative to the propeller for thrust generation is available at this small scale. An additional advantage of a flying wing is its robustness, but a critical point could be its reduced level of stability. For this reason a detailed stability analysis is required.

The parameters of the MAV-platform are optimised according to certain performance goals. The primary goal is a near to maximal endurance in cruise conditions. Additional constraints are the fact that the MAV should be stable and controllable without the need of active stabilisation equipment and it should be manoeuvrable. More specifically, it must be able to fly in urban terrain, which sets certain specific goals on turn radius and response time. Other requirements, which influence the final design, are payload modularity, component integration, robustness and simplicity.

The optimisation of the flight-time and the flight qualities of a MAV is impossible without the knowledge of the forces acting on the vehicle. Accurately estimating these forces is a challenging task because no experimental databases for low aspect ratio wings at low Reynolds numbers are available. Also, classical aerodynamic theory, which is an accurate predictive tool for the development of large-scale aircrafts, is not generally applicable for low aspect ratio wings at low Reynolds numbers. The aspect ratio (AR) of a MAV-wing is normally below two, which leads to complex three-dimensional flow. Because a MAV flies at low Reynolds numbers based on its wing chord (approximately between 5×10^4 and 2×10^5), complex flow phenomena such as laminar separation bubbles, laminar to

https://doi.org/10.1017/S0001924000004565 Published online by Cambridge University Press

Table 1
External parameters of a MAV

Wing	Propeller	Vertical tails	Control surfaces
wing profile	blade profile	number of tails	type
span	diameter	span	span
aspect ratio	chord distribution	aspect ratio	aspect ratio
planform	twist distribution	position on wing	position on wing
tip geometry	rotation speed		
	position		

Table 2
Flying wing aerofoils

Airfoil	Type	Camber (%)	t/c (%)	$C_{d,0}$	$C_{m,c/4}$
MH45	reflex	1·64	9·85	0·017	–0·006
N0009	symm	0	9	0·011	0
S5010	reflex	2·21	9·83	0·016	–0·007
S6063	semi-symm	1·43	7·05	0·01	–0·02
S8025	semi-symm	0·49	8	0·01	–0·003

turbulent transition and bubble bursting may arise. The comprehension of those complex phenomena and the development of numerical models to predict those forces are basic aspects of this research.

2.0 METHODOLOGY

Figure 1 shows a schematic outline of the methodology of the design process. The methodology basically consists of three levels: the basic level consists of the aerodynamic force models and profile selection, the second level is the multidisciplinary design optimisation and the third level consists of simulated flight testing (using Matlab/Simulink) and prototype test flights to test the flight qualities. These tests are used as a feedback module for the design method.

3.0 AERODYNAMIC MODELS

3.1 General approach

The subsystems that are subject to aerodynamic forces are the wing, the vertical tails, the propeller and the control surfaces. The construction of aerodynamic models that approximate the forces for a certain MAV configuration in any symmetrical or asymmetrical flight condition is the purpose of the first step of the design process.

It would be very time consuming and expensive to search for the best MAV configuration using experimental tests or CFD-computations alone. Limited accuracy of the experiments and limitations of the implemented turbulence and transition models of the CFD-models may even cast doubts on the value of such an optimisation procedure. A specific strategy is thus needed to estimate the forces using empirical and numerical models that can be validated using experimental data. A profound knowledge of all significant phenomena is needed. First of all, it is important to look for the different parameters that define one specific MAV configuration. Only parameters that influence external properties of the MAV are of any importance for the aerodynamic research. They are summarised in Table 1.

The wing is defined by a set of parameters. These parameters are the span, the aspect ratio, the planform, tip geometry and the profile. For reasons of simplicity, the use of twist is not considered as a design parameter. The use of dihedral is also not considered but it remains an option if it is necessary because of stability requirements. The optimisation of the tip geometry is an ongoing research topic as it has a significant influence on wing drag. The vertical tails are defined by geometrical aspects, their number and the position along the span of the wing surface. The propeller centreline is set on the centre chord of the wing. Parameters that influence the propeller forces are rotation speed, diameter, blade profile, twist distribution and chord distribution (and hub radius, though its influence is small and insignificant for the developed propellers). The distance between wing and propeller has a small impact on stability. Two common and simple configurations of the control surfaces are tested. The first configuration consists of a rudder on a central tail and an elevator. The second configuration consists of two elevons at the wing tips.

The different subsystems of the MAV will influence each other. It is important to understand these phenomena in order to estimate their effects on the aerodynamic forces. Slipstream effects of the propeller will have an impact on the wing, vertical tails and control surfaces. Upwash in front of the wing will influence the propeller forces. Wing geometry will have its impact on control surface effectiveness. The wing influences the forces on the vertical tails in asymmetrical flight because of sidewash; and vertical tails located towards the tip may influence the downwash distribution on the wing. The vertical tails will also influence each other. The force models of the MAV include analytical models of these effects or empirical models to estimate these effects. Numerical methods, such as vortex lattice methods, are used to investigate the influence of the wing on the control and tail surfaces.

3.2 Wing aerodynamics

A three-step approach is used to find the wing forces. First of all, a series of profiles is selected. These profiles are all low Reynolds number types selected from extensive experimental databases[7]. Many of those profiles do not show significant bubble drag and have an almost constant friction drag for low to moderate lift coefficients at Reynolds numbers as low as 100,000. Low Reynolds profiles are optimised for Reynolds numbers in the range [60,000-200,000] and have, on average, a thickness of about 8 to 9%. The primary selection criterion is the moment around the quarter point of the chord (aerodynamic centre). Only reflex (S-type) and (almost) symmetrical aerofoils have small enough moments to be considered as a possible flying wing profile. A selection of profiles that satisfy this criterion is listed below. The zero-lift drag coefficient and the moment coefficient around the quarter chord are also given (for $Re = 10^5$). An ideal aerofoil has a small nose-up (positive) moment at the aerodynamic centre that reduces the elevator trim angle, does not exhibit excessive low Reynolds bubble drag, has a trailing-edge thickness that can be manufactured and has a thickness distribution that satisfies the thickness constraints of the internal components. Such a profile was selected for the prototypes. The aerofoil is an adapted low Reynolds aerofoil with increased reflex.

In a next step, the primary aerodynamic forces of the wing are computed for a cruise condition (symmetrical and level flight). To optimise the endurance, it is important to accurately predict the drag, lift and the pitching moment of the wing. However, small aspect ratio wings at low Reynolds numbers are subject to unusual flow phenomena. The flow around the wing consists of a bound vortex and two tip vortices at the lateral edges. This bound vortex generates a linear lift component and an induced drag component. The viscous boundary layer of the bound vortex flow give rise to friction drag and pressure drag, which may be difficult to predict because of low Reynolds phenomena. At the lateral edges a shear layer is formed. It

https://doi.org/10.1017/S0001924000004565 Published online by Cambridge University Press

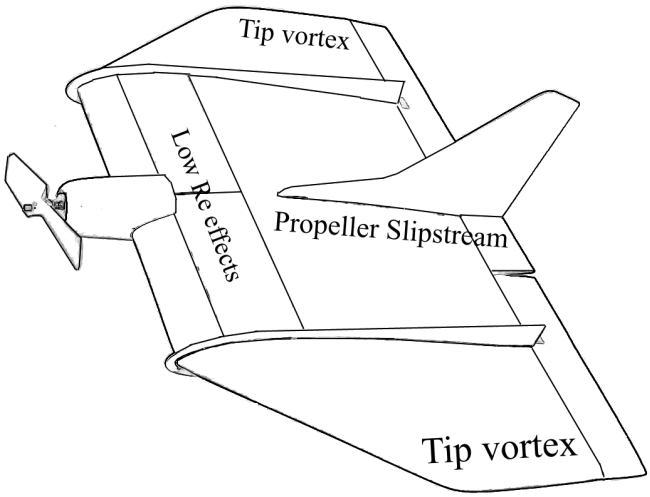


Figure 2. Special flow zones on the UGMAV25.

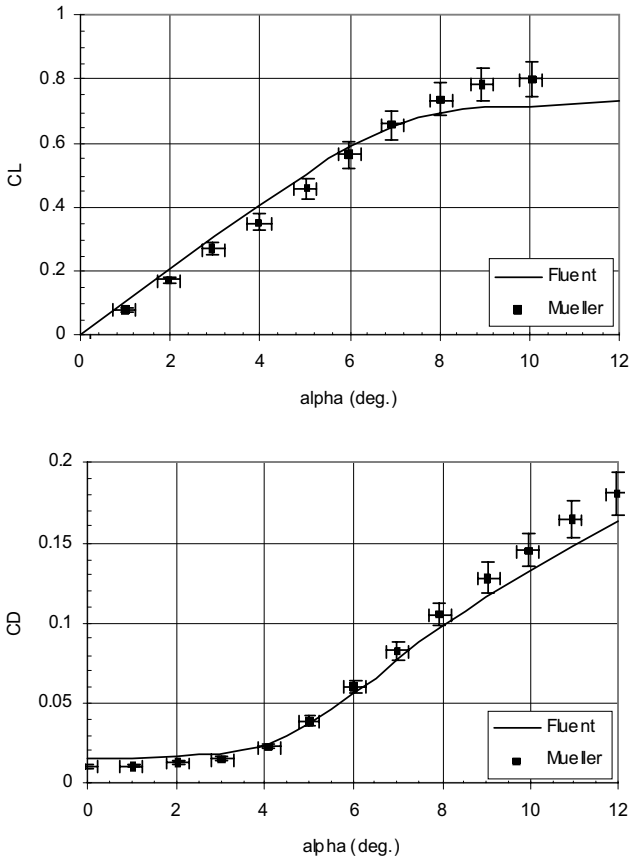


Figure 3. C_L and C_D of flat plate, 2D, $Re_w = 10^5$.

is unstable and starts rolling up the vortex sheet that leaves the wing. The vortices cover a part of the suction side at the tip and interact with the wing, increasing the local flow velocity and reducing the pressure. This secondary effect of the vortex sheet causes a non-linear drag and lift component, the vortex drag and vortex lift. A beneficial effect of these vortices is to reduce the impact of low Reynolds number effects (such as separation bubbles) on the wing. Some special zones on a MAV wing are illustrated in Fig. 2.

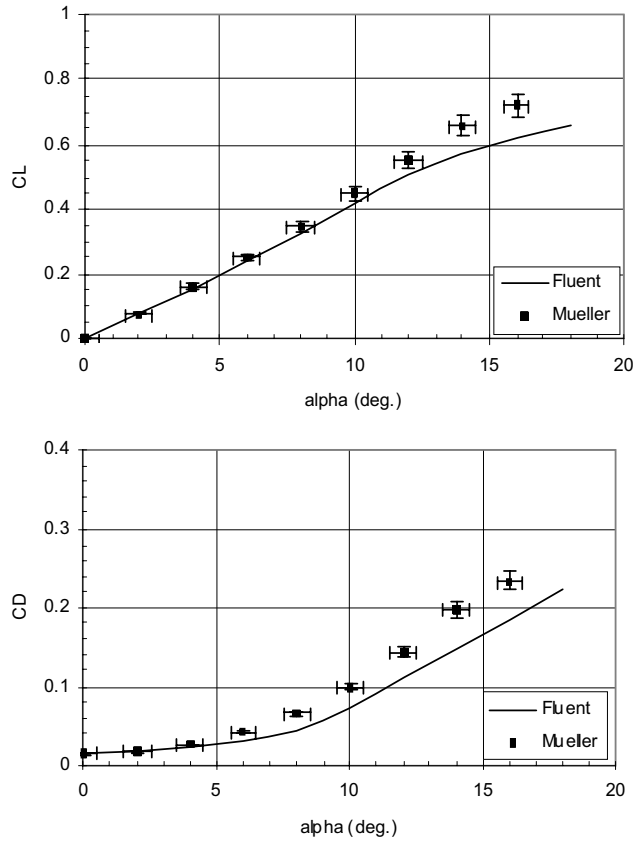


Figure 4. C_L and C_D of flat plate, AR = 1·5, $Re_w = 10^5$.

The linear lift for a certain planform and aspect ratio is computed using a vortex lattice method[8]. A strip method is used to find the drag components associated with the bound vortex. Based on the linear lift distribution along the span, the local effective angle of attack is computed and the local drag coefficient along a small strip (in chord wise direction) of the wing is found using 2D experimental data. The method has the benefit that it combines experimentally measured profile drag and induced drag for low aspect ratio wings for which the use of a lifting line approximation is inappropriate. By using 2D experimental drag, non-linear aerodynamic effects are also included. To find the vortex lift and drag, CFD computations were performed using a commercial code (Fluent Inc). The lift and drag data of the CFD-computations was first validated with experimental data. Figures 3 and 4 show the results of a flat plate profile and low aspect ratio wing (AR = 1·5) at $Re_w = 10^5$[9]. The flat plate has a thickness-to-chord ratio of 1·96%, a 5-to-1 elliptical leading edge and a sharp trailing edge. The results are compared with experimental data of Mueller[10] and Torres & Mueller[11].

An empirical formula, based on the theory of Polhamus[12] and Lamar[13], was used to fit the forces associated with the tip vortex as a function of the aspect ratio.

$$C_{L,vor} = K_v(AR)\mathrm{Cos}\alpha\mathrm{Sin}^2\alpha \quad \ldots (1)$$

$$C_{D,vor} = K_v(AR)\mathrm{Sin}^3\alpha \quad \ldots (2)$$

The total drag and lift is compared to existing low Reynolds data to validate the method[10,11,14]. The method is reliable as long as profiles are used which do not exhibit excessive low Reynolds effects. The strip method has the disadvantage that it over-predicts these effects at the tip sections if the tip vortices are strong simply because it does not include the tip vortex flow, which suppresses the low Reynolds

https://doi.org/10.1017/S0001924000004565 Published online by Cambridge University Press

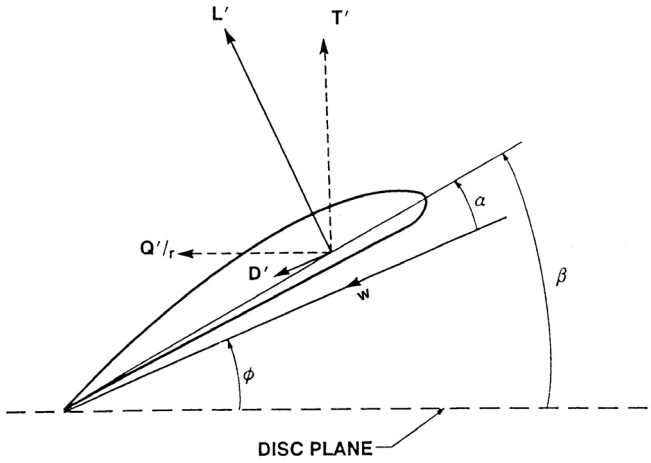


Figure 5. Propeller blade section.

effects at the wing tips. For the profiles considered, the force models are adequate for the optimisation studies.

The last step consists of a study of lateral and longitudinal stability derivatives of the wing. The longitudinal derivatives to the angle of attack are estimated or derived from the forces calculated in the previous step. The derivatives to the pitch rate are calculated using vortex lattice computations. The lateral stability derivatives are estimated using existing experimental data on low aspect ratio wings and empirical relations (e.g. Ref. 15). CFD simulations were used to predict the important derivatives to the side slip angle of the wing.

3.3 Propeller design

A rotating propeller with a certain number of blades (B) generates a thrust force (T) and a torque (Q) that needs to be countered by the torque of motor and gear. If the distribution along the radius (R) of the flow angle (ϕ), the blade twist angle (β), blade chord (c) and the velocity (w) is known as well as the blade section drag ($C_{d,blade}$) and lift ($C_{l,blade}$) as a function of the local angle-of-attack (α) then the thrust and torque can be derived (formulas are per unit radius):

$$T' = B\rho w^2 \pi r c\left(C_{l,blade}\mathrm{Cos}\phi - C_{d,blade}\mathrm{Sin}\phi\right) \quad \ldots (3)$$

$$Q' = B\rho w^2 \pi r^2 c\left(C_{d,blade}\mathrm{Cos}\phi + C_{l,blade}\mathrm{Sin}\phi\right) \quad \ldots (4)$$

To reduce the number of unknowns, design methods exist that optimise the propeller geometry for a certain axial free-stream velocity (V), thrust (or power input), radius and rotation speed (n). These methods are minimum induced loss methods, which means that they satisfy the Betz condition for minimum energy loss[16]. The Betz condition requires the vortex sheet of the propeller to be a regular screw surface; i.e., Tanϕ must be a constant independent of radius. Depending on the treatment of the axial flow and radial flow, different methods with increasing complexity exist[17-19]. The current research uses the method of Adkins and Liebeck[18] because of its accuracy and because of its moderate numerical cost in comparison with more time consuming models such as the helicoidal vortex models[19]. The method is valid as long as classical blade element analysis is applicable, which means that interaction between stream tubes are independent of one another. This is true for the developed propellers because they have a low disk loading. To reduce the computation time, the Prandtl function[16] for the radial momentum loss function was selected instead of a Goldstein function[20]. The impact of this simplification on the optimal propeller efficiency is considered to be insignificant.

The method minimises the momentum (induced) losses and minimises the viscous losses separately by setting the blade angle-of-attack corresponding to the minimum value of:

$$\varepsilon = \frac{C_{d,blade}}{C_{l,blade}} \quad \ldots (5)$$

Adkins and Liebeck proved that the optimisation of viscous and momentum losses are indeed uncoupled for high Reynolds number flows and an optimum is found (at least locally). Values of ε should be derived experimentally but a reasonable value is:

$$\varepsilon = \frac{5}{\sqrt{\mathrm{Re}_{blade}}} \quad \ldots (6)$$

Re_{blade} is the local Reynolds number. This relationship is derived using some simple relations. The local Reynolds number based on the propeller chord and local velocity is in the range 5,000-25,000, which means that a laminar flow regime exists. The laminar friction drag of a flat surface is:

$$C_{f,lam} = \frac{1{\cdot}328}{\sqrt{\mathrm{Re}_{blade}}} \quad \ldots (7)$$

For thin profiles with modest camber and a thickness ratio t/c, the profile drag can be estimated as:

$$C_{d,blade} = 2C_{f,lam}\left(1 + t/c\right) \quad \ldots (8)$$

This is a good estimation as long as drag divergence due to leading edge drag and separation can be avoided. Separation is certainly not a desired working point for an optimised propeller. With Equation (7) and Equation (8) ε becomes:

$$\varepsilon = \frac{2{\cdot}656\left(1 + t/c\right)}{C_{l,blade}\sqrt{\mathrm{Re}_{blade}}} \approx \frac{5}{\sqrt{\mathrm{Re}_{blade}}} \quad \ldots (9)$$

For the thin propeller blades used, the optimal value of $C_{l,blade}$ is about 0·5-0·6.

To analyse the results of the minimum induced loss method, it is useful to make the parameters dimensionless. If V, R, ρ, μ are used as a set of reference values, one can write for the thrust, power and rotation speed:

$$T_c = \frac{2T}{\rho V^2 \pi R^2} \quad \ldots 10)$$

$$P_c = \frac{2Q\Omega}{\rho V^3 \pi R^2} \quad \ldots (11)$$

$$\lambda = \frac{V}{R\Omega} \quad \ldots (12)$$

$$J = \frac{V}{Dn} = \pi\lambda \quad \ldots (13)$$

λ is the speed ratio, which relates the free-stream velocity to the tip speed of the propeller. More commonly the advance ratio (J) is used. The propeller efficiency can be written as:

$$\eta_{prop} = \frac{VT}{Q\Omega} = \frac{T_c}{P_c} \quad \ldots (14)$$

For a propeller with a given thrust, the propeller efficiency depends on the advance ratio, thrust coefficient (T_c) and a third non-dimensional group:

$$\mathrm{Re}_p = \frac{VR\rho}{\mu} \quad \ldots (15)$$

https://doi.org/10.1017/S0001924000004565 Published online by Cambridge University Press

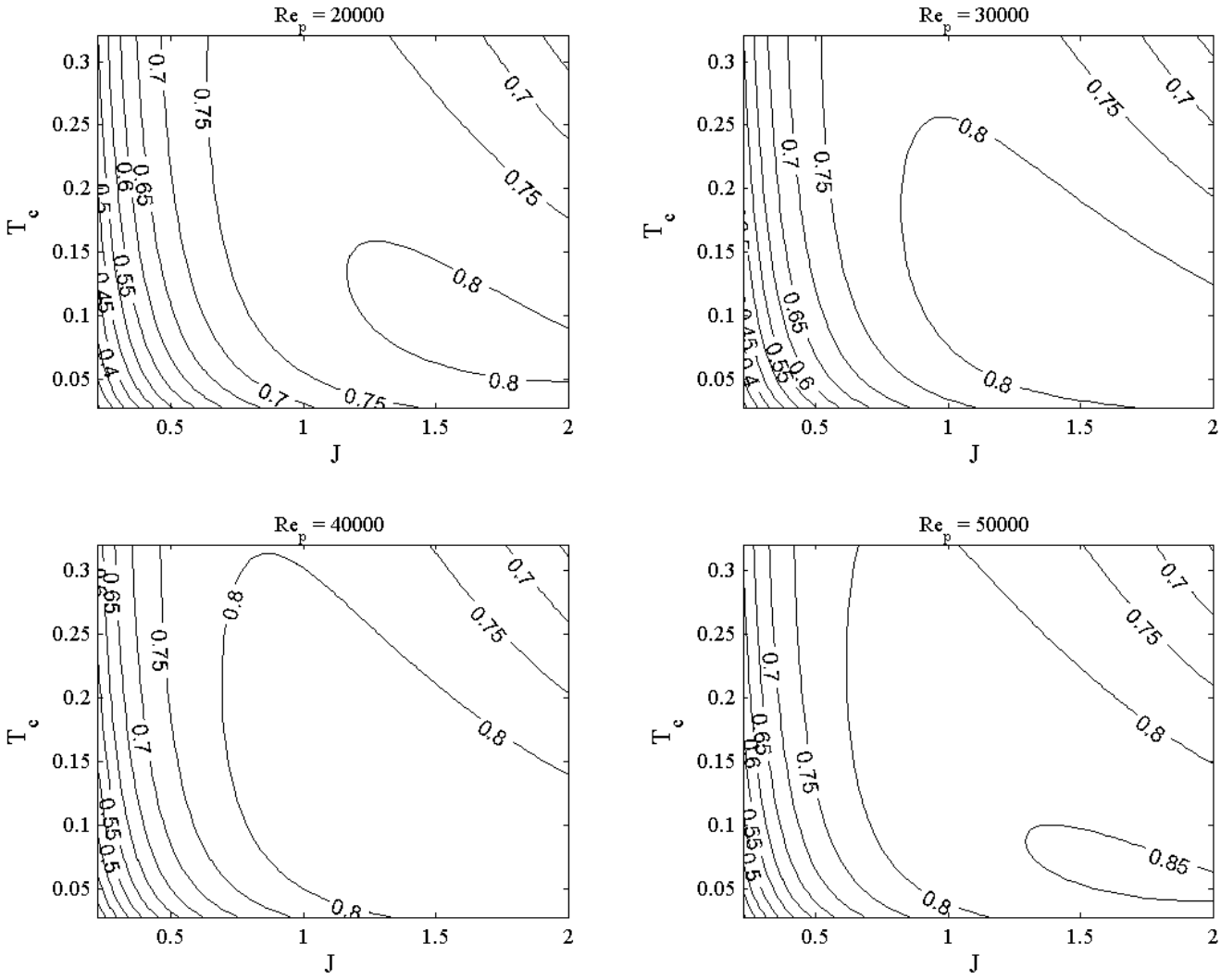


Figure 6. Propeller efficiency.

This representative Reynolds number depends on the product V and R and is for an optimised MAV in the range [20,000-60,000]. The lower range corresponds to light weight (slow flying) MAVs with a direct-drive transmission and the upper range to heavier MAVs with a transmission gear (larger propeller).

$$\eta_{prop} = f\left(T_c, J, \mathrm{Re}_p\right) \quad \ldots (16)$$

The propeller efficiency is only a function of three dimensionless groups. Eventually, a fourth group can be added which is the ratio of hub radius and propeller radius. In the case of MAVs, the hub radius is too small to have an impact on the optimal propeller efficiency. The Mach number is not important because the Mach number at the tip is <<1. Figure 6 shows the optimal propeller efficiency as a function of three nondimensional parameters (the hub radius is set to 1/20th of propeller radius):

The method is in good agreement with experimental data[18]. Also two propellers were designed with the same settings of the geared and direct drive propeller of the Black Widow[2]. A very similar geometry in comparison with the photographs of the propeller was obtained. The propeller efficiency was respectively 0·69 and 0·8, which is almost exact in agreement with the experimental data[2]. A similar design method was probably used to develop the propellers of the Black Widow.

Besides the thrust and torque, some other propeller-related parameters need to be derived. The flow attacks the propeller at a certain angle because the propeller is fixed along the centreline of the wing. This angle is the angle of attack increased by an induced upwash angle caused by the wing circulation, which depends on the position of the propeller in relation to the wing. As a result, there are two relatively small effects generated, a normal force and a yawing moment. The normal force and the yawing force can be estimated using blade element theory[14,21]. They have a limited influence on the stability derivatives and are not important for the endurance optimisation. Besides the propeller efficiency, there is also a secondary influence on the endurance because propeller-stream effects on the wing have an impact on the wing forces. To calculate these effects in advance, the propeller is modelled as an actuator disk and its effects on lift, drag and pitching moment are estimated using analytical approximations. In general terms one can say that the propeller increases the velocity (the dynamic pressure) and decreases slightly the angle-of-attack in the prop-wash zone.

https://doi.org/10.1017/S0001924000004565 Published online by Cambridge University Press

3.4 Aerodynamics of control surfaces

A model for the lift and pitching and rolling moment changes due to control surface deflection is derived using a model based on Hoerner[14] and Lowry and Polhamus[22].

$$\frac{dC_L}{d\delta} = \frac{dC_L}{d\alpha} \cdot \frac{d\alpha}{d\delta}\left(\frac{c_c}{c}\right) \cdot K_b\left(\frac{b_c}{b}\right) \quad \ldots (17)$$

$$\frac{dC_m}{d\delta} = \frac{dC_{m,0}}{d\delta}\left(\frac{c_c}{c}\right) \cdot K_b\left(\frac{b_c}{b}\right) \quad \ldots (18)$$

$$\frac{dC_l}{d\delta} = 2\frac{dC_L'}{d\alpha} \cdot \frac{d\alpha}{d\delta}\left(\frac{c_c}{c}\right) \cdot K_b\left(\frac{b_c}{b/2}\right)\frac{y_{ac}}{b/2} \quad \ldots (19)$$

$dC_L/d\alpha$ is the slope of the lift coefficient of the wing (elevator, elevon) or vertical tail (rudder); $d\alpha/d\delta$ is the effectiveness ratio, which is a function of the chord ratio (control surface chord c_c divided by wing chord c); K_b is the span-effectiveness that is a function of the span ratio of control surface span b_c and wing span b; $dC_{m,0}/d\delta$ is the pitching moment due to trailing edge deflection of a 2D aerofoil; $dC_L'/d\alpha$ is the slope of the lift coefficient of a wing with half the aspect ratio of the original wing and y_{ac} is the distance between the aerodynamic centre of one elevon and the centre chord of the wing.

An optimal control surface limits the negative effect on the lift (Equation (17)) for a desired value of $dC_m/d\delta$ (which will depend on the choice of the stability margin). Optimal values of the chord ratio are in the range [0·075-0·15]. The factor K_b directly affects manoeuvrability and depends on the mission. It is desirable to cover a large part of the span to improve the response time of the MAV on a signal input. A large span-ratio is also useful if the control surface has to be used as a high lift device to increase the turn radius (aileron-mode, rudder).

Inviscid computations were not accurate for the derivation of these force derivatives. Vortex-lattice computations of wing and control surface were also performed but $dC_L/d\delta$, $dC_m/d\delta$ and $dC_l/d\delta$ were all overpredicted, typically by 10-20%.

The control-surface models are useful for dynamic analyses. They don't have a significant impact on the endurance analysis because a good choice of the wing aerofoil and stability margin will set the trim condition of the vehicle in cruise condition at almost zero deflection angles. Of course, small angles are needed to take non-symmetrical effects of the propeller into account.

3.5 Aerodynamics of tail surfaces

Tail surfaces are crucial for lateral stability. A good estimation of the side force, yawing moment and rolling moment due to side slip angle, yaw rate and roll rate is a must. This totals nine stability derivatives that need to be estimated. The most important derivative is the side force due to sideslipping, as all other forces are directly proportional to this force. Normally, for a tail that is not influenced by the wing, all derivatives can be found using the side force due to side slip and the position of the wing's aerodynamic centre in relation to the centre of gravity (z' is the horizontal distance and x'' the vertical distance). The relations are given in Table 3. The nondimensional roll rate and yaw rate are used. The relations are valid for a right-handed body-fixed reference frame with the X-axis pointing towards nose and the Z-axis towards the bottom of the MAV. However, these relations give bad estimations if the ratio of tail chord and x' is very small (<0·2) and if the tail is influenced by sidewash of the wing, which is definitely the case for a vertical tail on a flying wing. Sidewash will make a part of the tail ineffective and even counter effective. In order to take these effects into account, wing and tail surfaces are analysed using a vortex lattice method[8]. The stability derivatives are computed around a reference point. By subtracting the stability derivatives of the wing without tails, an estimation of the stability derivatives of the tails alone are found including the sidewash of the wing. The computed lateral stability derivatives of the wing are excluded because it was found that the lateral derivatives of the wing computed with the vortex lattice method were not well predicted. These are computed using empirical relations and CFD simulations as described in the wing aerodynamics section.

Table 3
Stability derivatives of an isolated vertical tail surface

	Side force Y	Rolling moment l	Yawing moment n
Side slip β	Y_β	$z' \cdot Y_\beta$	$-x' \cdot Y_\beta$
Roll rate p	$2z' \cdot Y_\beta$	$2z'^2 \cdot Y_\beta$	$-2z'x' \cdot Y_\beta$
Yaw rate r	$-2x' \cdot Y_\beta$	$-2z'x' \cdot Y_\beta$	$2x'^2 \cdot Y_\beta$

4.0 MULTIDISCIPLINARY DESIGN OPTIMISATION

Once the aerodynamic forces of the subsystems can be derived for any MAV configuration, optimisation studies are the next step in the development of a MAV-platform. The developed multidisciplinary design optimisation (MDO) finds the optimal parameters of a MAV with a certain weight and span. Technological constraints limit the size and weight reduction of the internal components and set a lower limit on the mass of the vehicle for a certain span.

The MDO optimisation consists of three parts: an endurance optimisation, which is the general optimisation routine of the wing and propeller, a component selection analysis to find the internal components and a dynamic analysis, which optimises the tail surfaces, the control surfaces and analyses the effect of parameters such as wing sweep and centre of gravity. A detailed approach will require iterations, as there is a clear mutual influence between the difference optimisation routines.

4.1 Endurance optimisation and component selection

The primary objective of the multidisciplinary design optimisation is to find the MAV configuration that has the longest endurance for a certain span and a certain amount of payload mass. Because both the wing and propeller aerodynamics depends on the cruise conditions and because they influence each other, wing optimisation and propeller optimisation are coupled and should be optimised together. The motor may also play an important role because, normally, the motor has a direct-drive transmission or a fixed gear that sets limits on the propeller speed range (actually, the speed range is not limited but the motor efficiency may have a dominant influence if it becomes too small).

To find an optimum configuration, a numerical approach is needed. The different subsystems (wing, motor, propeller) and force models are implemented in Matlab and different configurations of the MAV were tested to find close-to-optimum configurations for a MAV with a certain mass and span. A simplified analysis of the endurance is given below followed by some numerical results of a 25cm MAV.

4.1.1 The endurance formula

The endurance of a MAV is the total amount of available energy divided by the power consumption (m_{bat} is the battery mass, C_{bat} the energy density of the battery):

https://doi.org/10.1017/S0001924000004565 Published online by Cambridge University Press

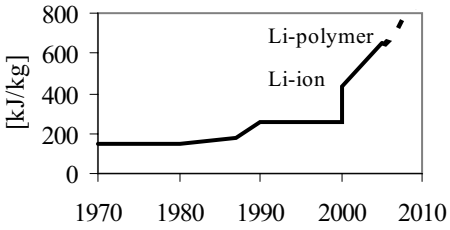


Figure 7. Historic trend in specific energy (C_{bat}).

$$E = \frac{C_{bat} m_{bat}}{P_{bat}} \quad \ldots (20)$$

The power delivered by the battery can be written as the power needed for the displacement of the vehicle, which is the velocity (V) times the drag (D), divided by the efficiency of the propulsion system, plus the power needed for other electronic devices (P_{dev}):

$$P_{bat} = \frac{V \cdot D}{\eta} + P_{dev} \quad \ldots (21)$$

The power needed for control system and control signal transmission is normally small in comparison with the power consumption of the motor. In some specific cases P_{dev} can be significant, for example if continuous broadband transmission is needed. We will focus on the power consumed by the propulsion system.

In cruise conditions the vehicle is in an equilibrium state. For a general MAV, with the motor aligned with the zero-lift angle, we get the following equilibrium condition:

$$\begin{aligned} T \cdot \mathrm{Cos}(\alpha) - D &= 0 \\ T \cdot \mathrm{Sin}(\alpha) + L - W &= 0 \end{aligned} \quad \ldots (22)$$

Using Equation (21), Equation (22) and the general definitions of lift and drag coefficient, the power can be written as:

$$P_{bat} = \frac{C_D}{\left(C_L + C_D \cdot \mathrm{Tan}\alpha\right)^{3/2} S^{1/2} \eta} W^{3/2} \left(\frac{2}{\rho}\right)^{1/2} \quad \ldots (23)$$

S is the surface area of the wing and ρ is the air density. Using Equation (20), Equation (23) and the following definitions of aspect ratio, $AR = b^2/S$, and weight, $W = g.m_{tot} = g.(m_{bat} + m_{rem})$, this leads to:

$$E = \left\{C_{bat}\right\} \left\{ \frac{m_{bat}}{\left(m_{bat} + m_{rem}\right)^{3/2}} \right\} \cdot \left\{ \eta b \frac{\left(C_L + C_D \mathrm{Tan}\alpha\right)^{3/2}}{C_D \sqrt{AR}} \right\} \left\{ \frac{\sqrt{\rho}}{g^{3/2}\sqrt{2}} \right\} \quad \ldots (24)$$

m_{rem} is the mass of the vehicle without batteries. For illustrative reasons, the different influences on the endurance are grouped using parentheses. These groups consist of the battery energy density, a battery mass-factor, the aerodynamic-factor that depends on wing aerodynamics and propulsive efficiency and an atmospheric factor. The first three factors can be optimised as discussed below.

4.1.2 Battery energy density

Currently, lithium-polymer batteries are the energy source with the highest energy density for MAVs. They are a logic choice as they are rechargeable without noticeable memory effect, they have the highest battery energy density to date, they are very thin and they are affordable because of mass-production. The lithium-polymer battery is a commercial off the shelf (COTS) component. The commercial trend in rechargeable batteries leads to a steady increase in the specific energy combined with a useful specific power. The development of increasingly lighter and smaller electronic devices such as mobile phones and PDAs are the main drivers behind this trend.

Eventually other energy sources such as fuel cells and micro-turbines may replace batteries as the energy source for MAVs. Figure 7 shows the current trend in the specific energy.

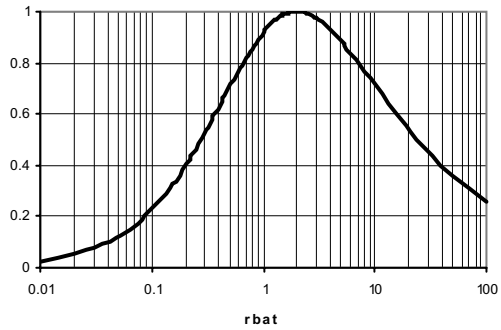


Figure 8. Normalised mass-factor.

4.1.3 Battery mass

Equation (24) clearly shows the importance of the battery mass on endurance, which reaches an optimum at a certain mass. However, Equation (24) is a simplification and, in reality, propeller efficiency and drag coefficient depend on the total mass and hence also on battery mass for a certain MAV with a given span (albeit that those effects are small). They are a result of the fact that similar MAV configurations with higher masses need to fly at higher velocities (and higher propeller speeds) and are hence at a higher Reynolds number, increasing slightly the propulsive efficiency and decreasing the drag coefficient. If those small effects are neglected one can find an optimum for the battery mass. The optimal battery mass is derived by:

$$\frac{r_{bat}}{\left(1 + r_{bat}\right)^{3/2}} \cdot \frac{1}{\sqrt{m_{rem}}} \quad \ldots (25)$$

Which gives:

$$m_{bat} = 2m_{rem} = \frac{2}{3} m_{tot}$$

If the following relation is used: $m_{bat} = r_{bat} m_{rem}$, the mass-factor becomes:

$$\frac{r_{bat}}{\left(1 + r_{bat}\right)^{3/2}} \cdot \frac{1}{\sqrt{m_{rem}}} \quad \ldots (26)$$

As expected, the mass of the remainder should be minimised. It consists of a user-defined amount (payload mass) and the mass of essential components such as the propulsion system and the structure. r_{bat} should be close to its optimum, which is two. Figure 8 shows a normalised r_{bat}-factor as a function of r_{bat}. If one takes the Reynolds number effects into account, the optimum battery mass should be slightly higher. So, according to this theory, it's no surprise that the battery mass of the WASP has a battery mass that amounts to 70% of the total mass. The WASP is a 13 inch span mini unmanned air vehicle build by Aerovironment, which has currently the endurance record at this scale. For smaller MAVs, a battery mass that equals 50% of the total mass may be easier to achieve and still gives an adequate endurance of 92% of the optimum.

https://doi.org/10.1017/S0001924000004565 Published online by Cambridge University Press

Table 4
Motor data

$k\phi$	0·002V/rps
M_0	0·06 mNm
R_{mot}	0·02 O
I_{max}	1 A
N_{max}	350rps

4.1.4 Propulsive efficiency

The propulsive efficiency can be written as a product of propeller efficiency, gear efficiency and motor efficiency:

$$\eta = \eta_{prop}\eta_{gear}\eta_{mot} \quad \ldots (27)$$

In an ideal situation, wing and propeller optimisation are decoupled from motor optimisation. Optimal motor speed and optimal propeller speed can be set separately if there is no limitation on the gear ratio. Unfortunately this is not the case, only certain ratios are available. Moreover, the addition of a gear leads to an additional loss, which is not negligible ($\eta_{gear} \sim 0{\cdot}85$ for a 1:4 transmission at this scale), and increases the weight by a few grams. Because slow rotating propellers need a larger diameter, the propeller mass and inertial moment may become important also. The mechanical time constant of a DC motor is proportional with the moment of inertia of propeller and rotor. The propeller efficiency was discussed in the section about propeller design; the motor efficiency is discussed below.

4.1.5 Motor design

A motor that fits the optimised propeller and MAV needs to deliver the needed torque M at a maximal efficiency. The motor efficiency can be formulated as:

$$\eta_{mot} = \frac{\Omega_{mot} M}{UI} = \frac{2\pi n_{mot} M}{UI} \quad \ldots (28)$$

The relationships between speed/torque (Ω_{mot}/M) and voltage/current (U/I) are:

$$U = k\phi\Omega_{mot} + R_{mot} I \quad \ldots (29)$$

$$I = \frac{M}{k\phi} + I_0 = \frac{M + M_0}{k\phi} \quad \ldots (30)$$

$k\phi\Omega_{mot}$ is the electromotive force, which depends on the speed, flux and winding. M_0 is a friction moment. A specific motor type has normally a series of $k\phi$ values, which choice depends on the application. The relationship between M and Ω_{mot} is:

$$\Omega = \Omega_0 - \frac{R_{mot}}{(k\phi)^2}(M + M_0) \text{ and } \Omega_0 = \frac{U}{k\phi} \quad \ldots (31)$$

For a specific Ω_0 the optimum is found as:

$$\eta_{mot,opt} = \left(1 - \sqrt{\frac{M_0 R_{mot}}{\Omega_0 (k\phi)^2}}\right)^2 \quad \ldots (32)$$

An optimal motor has a minimal value of $R_{mot}/(k\phi)^2$ and a limited value of $M_0(<<M)$. These values are technology specific and normally depend on the temperature of the motor (which depends on the generated heat and hence the current). For a specific motor type, only Ω_0 is a free parameter that influences the maximum motor efficiency. For a system with a direct-drive propeller it is directly related to a choice of the advance ratio J, and hence the propeller optimisation. Figure 9 gives the motor efficiency for a representative MAV-motor (see Table 4 for motor data):

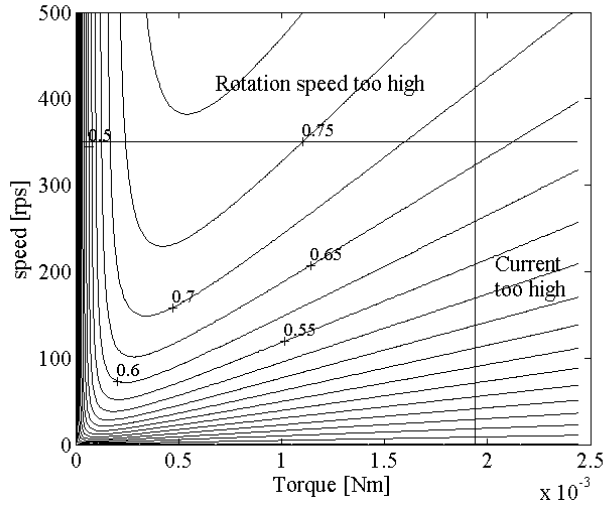


Figure 9. Motor efficiency as a function of n [rps] and M [Nm].

The maximal values of I (a thermal constraint) and n (a mechanical constraint) are normally the boundaries within the workable range for a specific motor. The maximum efficiency is obtained at the maximal allowable rotation speed. A problem regarding small motors is the fact that the maximal motor efficiencies attainable decrease with decreasing mass of the motor. The reasons are primary mechanical construction limitations (tolerances, forces on bearing) and heating issues. For example, a 50g motor has a maximum efficiency that is 10% higher then a 10g motor. In order to reach the maximum efficiency of a small motor (~ 80%), the rotation speed must be very high (350rps). This leads to low optimum values of J and, as a result, low propeller efficiencies. The use of a gear is not always an option and may not be very beneficial because of limited transmission efficiency. Taking all these limitations in to account, the maximal attainable propulsive efficiency of a MAV is currently in the order of 50-55%.

Besides the motor efficiency, three additional important aspects are its available power, its mass and its diameter. In order to have a manoeuvrable vehicle, the excess power in cruise conditions should be significant. The excess power is defined as the maximum available power minus the necessary amount of power (Equation 23). The amount of excess power is mission-specific and depends on manoeuvrability constraints such as minimum climb angle and turn radius at cruise conditions and/or off-design conditions. The mass is important because it is a significant contribution to the total mass. For a MAV of 15-25cm, the mass is in the 10-25g range, which is normally about 10-15% of the total mass. The diameter of the motor is important because the motor is normally the thickest component. The motor thickness sets a limit on the aspect ratio for a certain planform and profile combination. If it is not integrated in the wing, it may generate a significant protuberance drag.

4.1.6 Numerical endurance analysis

A computer code was written to find the cruise condition of a MAV with a certain span and weight. This code includes the aerodynamic wing models, the equilibrium state equations, a propeller optimisation code, a motor model with an integrated thermal model, simulation of the prop-wash effects, etc. Figure 10 shows the results for a MAV with the same wing as the UGMAV25 (details see Table 6), a direct-drive propulsion system with motor characteristics comparable with those of Table 4 and a total mass in the range [10-

https://doi.org/10.1017/S0001924000004565 Published online by Cambridge University Press

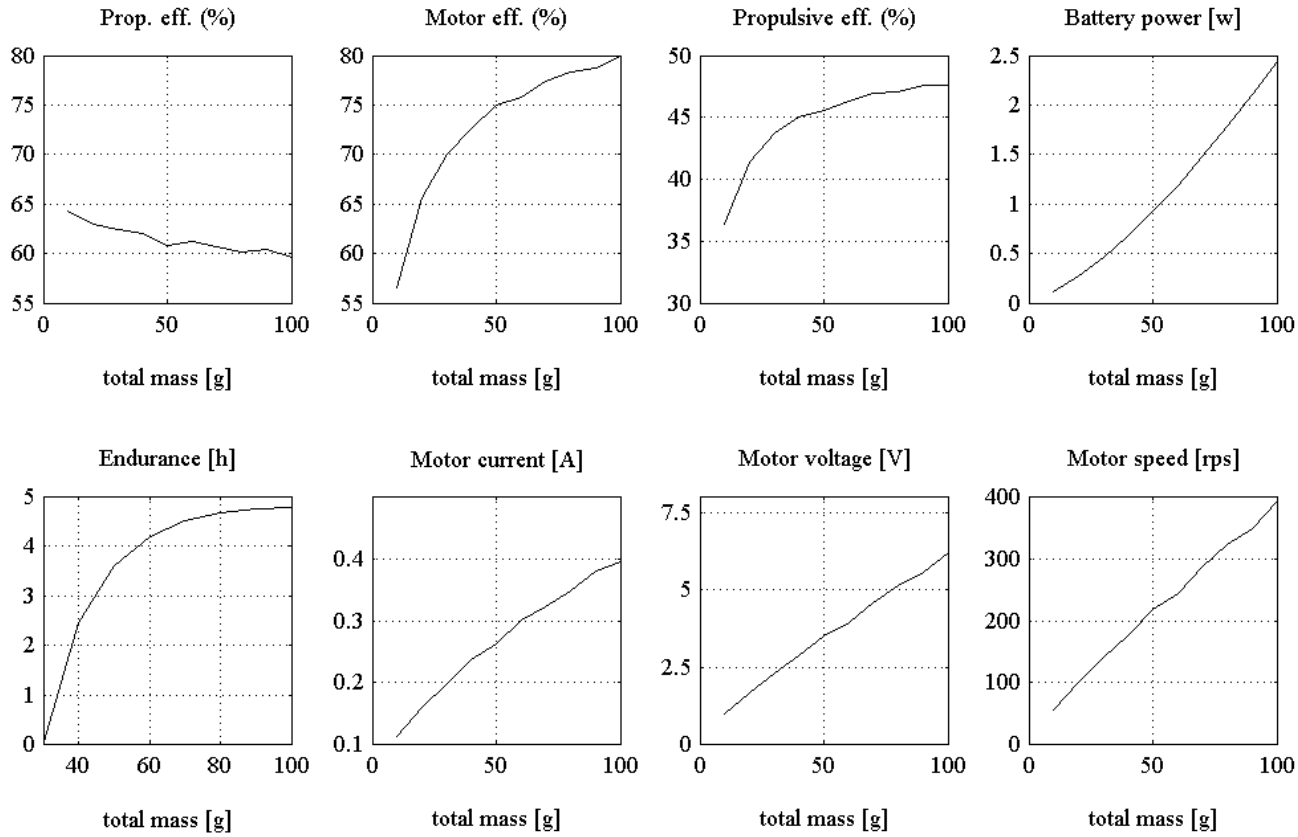


Figure 10. Results of the numerical endurance optimisation.

100g]. The endurance is derived for a remainder mass of 30g and a specific energy density of 600kJ/kg. The maximum endurance is found for a total mass of 90g, as predicted by the theory. The high endurance is the absolute maximum in a perfect and constant cruise condition without any additional battery losses due to the energy consumption of other components. Of course, in reality other components may consume a significant amount of energy. For example, a transmitter of a video signal may easily consume 0·5w of energy. An additional critical point is the low Reynolds number behaviour. 2D data of the profiles considered is only available above Re_w ~ [60,000-100,000]. Extrapolations have been made to include lower Reynolds numbers. For this reason, one needs to be cautious with the results for low total mass values.

4.2 Dynamic analysis

A dynamic analysis is performed to find the remaining parameters and to analyse the flight qualities of the vehicle, which are the stability, controllability and manoeuvrability of the MAV. The primary objective is to find a stable and controllable vehicle.

Table 5
Stability modes of a MAV

	Eigenvalue	Damping	Freq (rad/s)
Short period	–22·7+33·1*i*	0·566	40·2
Phugoid	–0·19+1·53*i*	0·125	1·54
Roll	–13·2	-	-
Spiral	–0·14	-	-
Dutch roll	–6·2+27·7*i*	0·218	28·4

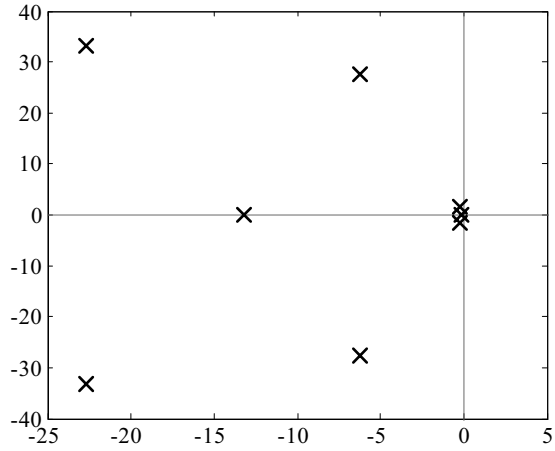


Figure 11. Stability modes of a MAV (eigenvalues).

The longitudinal modes and lateral modes are studied using the general equations of motion linearised around the cruise conditions. The free parameter for the longitudinal analysis is the static margin. The vertical tails, dihedral angle and sweep angle are free parameters of the lateral analysis. Sweep is almost a free parameter because planform influence on endurance is insignificant (as long as the average mid-chord sweep angle is below 45 degrees). An example of the different eigenvalues of the modes is given in Fig. 11 and Table 5. The frequencies are given in rad/s. The dynamic modes are computed for a 25cm MAV with a mass of 58g and two vertical fins with a total area of 20% of the wing surface area.

https://doi.org/10.1017/S0001924000004565 Published online by Cambridge University Press

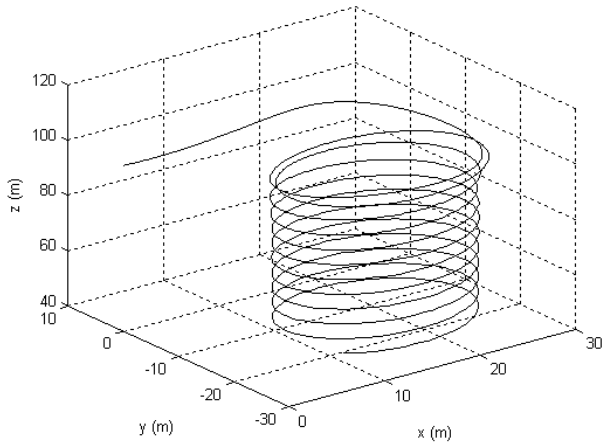


Figure 12. Simulated trajectory.



Figure 13. UGMAV25.

4.3 Some conclusions:

1. The short period mode and roll mode are dampened very fast.
2. The dutch roll mode has a fast 4·5Hz oscillation. The damping factor depends on the tail area.
3. The phugoid mode is a slow dampened mode. The damping factor is increased if the C_D/C_L ratio is increased but this ratio is imposed by the endurance optimisation. There is also an influence of the propulsion system.
4. The spiral mode is slightly dampened. An increase in wing sweep makes it more stable.

The controllability of the vehicle depends on the control system. It is important to look at the modes triggered by the control system. Too much oscillation should be avoided. Based on the stability study one can conclude that a system with two elevons is better than a rudder and elevator. The later configuration requires an active control system (yaw-damper) to damp the Dutch roll mode[2]. A rudder-elevator system has also the disadvantage that it leads to a less manoeuvrable vehicle with a larger minimal turn-radius. Normally, a rudder isn't primarily used to turn. The main purpose of the rudder is to offset adverse yaw caused by a deflection of the ailerons/elevons and to quickly balance against crosswinds. A camera-platform with minimal yaw errors may be an advantage for certain missions but in urban terrain the ability to turn may be critical. So, the choice of the control system is mission-specific.

The vertical tail volume coefficient C_{VT} can be used to find a decent value for the vertical tail area (S_{VT}). l_{VT} is the distance between the aerodynamic centres of wing and tail:

$$C_{VT} = \frac{l_{VT} S_{VT}}{bS} \quad \ldots (33)$$

The dynamic analyses and flight tests showed that the vertical tail volume coefficient of a MAV should be around 0·05-0·06. This ratio is in-between the value for general aviation aircraft (0·04) and jet fighters (0·07).

Table 6
Properties of the UGMAV25

Span	25m
Aspect ratio	1·8
Wing area	347cm^2
Taper	0·5
Tail area	48·5cm^2
Wing thickness to chord ratio	10·5

5.0 SIMULATIONS AND PROTOTYPE

A complete simulator of the flight dynamics and a 25cm prototype was developed based on the force models and design parameters of the MAV design method. The simulated and real flight tests are used as feedback to optimise the design method and to find unexpected behaviour.

5.1 Flight simulations

Non-linear simulations of the MAV dynamics were performed using the Flight Dynamics and Control toolbox (FDC toolbox) for Matlab/Simulink[23]. The toolbox was written by Marc Rauw and implemented for the Beaver airplane. Changes in the engine model, the aerodynamic force models and the control inputs were needed for the MAV. The simulations were useful to analyse in more detail the flight qualities and stability modes in any flight situation. For the latter analysis, a linearisation routine was written in Matlab to linearise the motions around any state. The simulink-model of the MAV-dynamics is also used for the first development phase of an autonomous MAV. Figure 12 shows a trajectory of a MAV that gets an aileron input and goes in circular flight.

5.2 Prototype

The first prototype that was developed using the design method was the UGMAV25 (Fig. 13), with a span of 25cm. It was mainly designed to test the stability and controllability. To reduce the total mass and hence the flight velocity, this configuration uses a small battery pack (145mAh, 7·4 V). The first test flight turned out to be very successful. The MAV was hand-launched using a central surface grip at the bottom, located at the centre of mass. The vehicle was stable and performed a series of acrobatic flight manoeuvres. The total flight time of this vehicle was 17 minutes flying mostly at full throttle, performing medium and steep turns. To protect the motor, the current was limited to 1 ampere. The robust structure of the vehicle allowed landing without damage. Table 6 gives some design parameters.

The batteries used are lithium-polymer batteries (Kokam 145). The UGMAV25 doesn't use the propeller of the design method but a commercially available propeller. This has a negative effect on the efficiency of the propulsion system (the efficiency is estimated to be around 25%) but the endurance was not the objective of the test. The production, experimental testing and verification of designed propellers is a topic of current and future research work.

https://doi.org/10.1017/S0001924000004565 Published online by Cambridge University Press

Table 7
Mass breakdown of the MAV

Structure	14g
Propulsion system	12g
Batteries	14g
Receiver - ESC - servos	18g
Total	**58g**

To control the vehicle, two small servos are used (type: Hitec HS55), a pico-reveiver (35MHZ) and an electronic speed control to control the coreless DC-motor. A normal antenna wire is used (50cm). Newer prototypes use a piano-wire or carbon antenna.

The control system is adequate for the flight tests but it is too limited for a real MAV. Besides the need for an autonomous control that limits the need of human remote control, the communication architecture has its limitations. The small size of the MAV and limited power to support the bandwidth available leads to a weak signal and the need of a powerful directional ground antenna that uses line-of-sight transmission. However, such a RF-link isn't useful for urban operations. The solution may be the use of a cellular communication architecture. For examples, existing and future mobile cell phone network services such as GPRS and UMTS maybe a solution, depending on the needed bandwidth (e.g. real-time video transmission *versus* bandwidth related to control functions). These issues are researched in a next phase in which the current MAV-platform is upgraded to an autonomous MAV. But, at this point, the autonomous control equipment is considered as a dummy mass.

A foam structure was used to make the wing of the prototype. Next-generation prototypes have a plastic shell structure. The latter one is a little lighter and less vulnerable but is more complex to build. The wing has a simple geometry and no dihedral. The masses of the components are summed up in Table 7. A smaller MAV, the UGMAV15, with a wings span of 15cm is currently under development.

6.0 CONCLUSIONS

A design method for micro air vehicles is developed. The emphasis lies on the design of a MAV-platform that includes only the most essential components. Using an analytical approach, all parameters of a MAV with a given span and payload mass can be derived. The method consists of different steps.

First the aerodynamic forces are derived for any MAV configuration for a given span. The method relies on aerodynamic force models for the four external subsystems of the MAV, which are the wing, the propeller, the vertical tails and the control surfaces. The force models are based on linear numerical methods such as a vortex lattice method, empirical models and optimisation theories. CFD and experimental 2D data were used to include non-linear effects such as tip vortices and low Reynolds number effects.

In a next step a multidisciplinary design optimisation was used to derive the parameters. A maximum endurance was the primary objective. However, there were some specific constraints. The MAV needs to be stable without active stabilisation equipment and it needs to be controllable and manoeuvrable to fly in urban terrain. Primary endurance related parameters were selected based on an endurance optimisation and an analysis of the properties of the internal components. These include wing parameters such as the aspect ratio, profile and planform and other parameters such as the optimal battery mass and the propeller geometry. The remaining parameters were selected using a dynamic analysis. These consist of the vertical tails, the control surfaces, the centre of gravity and some wing angles (dihedral, sweep).

A non-linear simulation of the MAV dynamics was performed as a feedback for the design method. A prototype, the UGMAV25, with a 25cm span was constructed and successfully tested. The simulations and test flights showed that the design method is successful in selecting the different parameters of the MAV. Other prototypes with spans as low as 15cm are being tested.

ACKNOWLEDGEMENTS

The authors want to thank Rik Verbiest for his work in constructing and piloting the prototypes. Thanks to his practical knowledge on RC-aircraft, the MAVs could be constructed in a fast and accurate way. The research is supported by the Special Research Fund of Ghent University (BOF2002/DRMAN/052).

REFERENCES

1. MCMICHAEL, J. Micro Air Vehicles, 1998, DARPA briefing at the DUSD (S&T) Seminar on Emerging Technologies: Micro Air Vehicles, 11 December 1998, Alexandria, VA.
2. GRASMEYER, J.M. and KEENNON, M.T. AeroVironment, Inc. Development of the Black Widow micro air vehicle, 2001, AIAA-2001-0127, 39th Aerospace Sciences Meeting and Exhibition, 8-11 January 2001, Reno, NV.
3. KELLOGG, J. *ET AL* The NRL Mite air vehicle, 2001, Proceedings of the 16th International Conference on Unmanned Air Vehicle Systems, Bristol, UK, pp 25-1-25-14.
4. IFJU, P.G., JENKINS, D.A., ETTINGER, S., LIAN, Y., SHYY, W. and WASZAK, M.R. Flexible-wing-based Micro Air Vehicles, 2992, AIAA-2002-705, 40th AIAA Aerospace Sciences Meeting and Exhibition, 14-17 January 2002, Reno, NV.
5. SHYY, W., BERG, M. and LJUNGQVIST, D. Flapping and flexible wings for biological and micro air vehicles, *Progress in Aerospace Sci*, 1999, **36**, pp 455-505.
6. BOHORQUEZ, F., RANKINS, F. and BAEDER, J. Hover performance of rotor blades at low Reynolds numbers for rotary wing micro air vehicles, an experimental and CFD study, 2003, AIAA-2003-3930, 21st AIAA Applied Aerodynamics Conference, 23-26 June 2003, Orlando, FL.
7. SELIG, M.S. *Summary of Low-Speed Aerofoil Data* (Vol 1-3), 1997, University of Illinois at Urbana-Champaign, Soartech Publications, Virginia Beach, VA.
8. MELIN, T. A vortex lattice MATLAB implementation for linear aerodynamic wing applications, TORNADO release 1.23b, Royal Institute of Technology KTH, Stockholm, Sweden.
9. COSYN, P. and VIERENDEELS, J. Numerical investigation of low aspect ratio wings at low Reynolds numbers, *J Aircr*, 2006, **43**, (3), pp 713-722.
10. MUELLER, T.J. Aerodynamic measurements at low Reynolds numbers for fixed wing micro aerial vehicles, 1999, RTO AVT/VKI Special Course on Development and Operation of UAVs for Military and Civil Applications, 13-17 September 1999, VKI, Belgium.
11. TORRES, G.E. and MUELLER, T.J. University of Notre Dame, Low-aspect-ratio wing aerodynamics at low Reynolds numbers, *AIAA J*, 2004, **42**, (5), pp 865-873.
12. POLHAMUS, E.C. Predictions of vortex-lift characteristics by a leading-edge-suction analogy, *J Aircr*, 1971, **8**, (4), pp 193-199.
13. LAMAR, J.E. Extension of leading-edge-suction analogy to wings with separated flow around the side edges at subsonic speeds, 1974, NASA TR R-428.
14. HOERNER, S.F. and BORST, H.V. Fluid-dynamic lift, *Hoerner Fluid Dynamics*, 1975, Chapter 9 and Chapter 17, Brick Town, NJ.
15. CAMPBELL, J.P. and MCKINNEY, O.M. Summary of methods for calculating dynamic lateral stability and response and for estimating lateral stability derivatives, 1951, NACA Technical Note 2409.
16. BETZ, A. with appendix by PRANDTL, L. *Screw Propellers with Minimum Energy Loss*, 1919, pp 193-213, Gottingen Reports.
17. LARRABEE, E. Practical design of minimum induced loss propellers, April 1979, Society of Automotive Engineers, Business Aircraft Meeting and Exposition, Wichita, KS.
18. ADKINS, C.N. and LIEBECK, R.H. Design of optimum propellers, *J Propulsion and Power*, 1994, **10**, (5), pp 676-682.
19. CHATTOT, J-J. Optimization of propellers using helicoidal vortex model, *Computational Fluid Dynamics J*, 2002, **10**, (4), pp 429-438.
20. GOLDSTEIN, S. On the vortex theory of screw propellers, Proceedings of the Royal Society of London, 1929, Series A, **123**, pp 440-465.
21. RIBNER, H.S. Propellers in yaw, 1945, NACA report 820.
22. LOWRY, J.G. and POLHAMUS, E.C. A method for predicting lift increments due to flap deflection at low angles of attack in incompressible flow, 1957, NACA Technical Note 3911.
23. RAUW, M. *FDC 1.3 – A Simulink/Matlab Toolbox for Flight Dynamics and Control Analysis*, 2002, Dutchroll Software.

https://doi.org/10.1017/S0001924000004565 Published online by Cambridge University Press